Article

Additive Manufacturing by the Selective Paste Intrusion Method: Effect of the Distance of the Print NozzIe to the Particle bed on the Print Quality

A. Straßer[1*][0000-0003-0293-3392], **A. Haynack**[1][0000-0003-2262-6111], **T. Kränkel**[1][0000-0002-5650-3825], **and C. Gehlen**[1][0000-0002-1214-3960]

[1] Technical University of Munich, TUM School of Engineering and Design, Chair of Materials Science and Testing; Centre for Building Materials (cbm)

* Correspondence: alexander.strasser@tum.de

Abstract: The Selective Paste Intrusion (SPI) method is a layer-by-layer additive manufacturing technique that allows for the production of complex geometries in concrete elements by selectively bonding aggregates with cement paste in a particle bed. To create reinforced concrete, the Wire and Arc Additive Manufacturing (WAAM) process shall be integrated into SPI. This technique allows the production of almost free-formed reinforcement and thus complements the advantage of SPI to produce free-formed structures of almost any geometry. However, integration of WAAM into SPI poses a considerable challenge, as high temperatures are generated during the welding process. These temperatures can negatively affect the rheological properties of the cement paste, in turn the penetration behavior of the paste in the particle bed and, subsequently, the mechanical properties of the hardened concrete. A possible passive cooling strategy is to increase the protruding length of the reinforcement bars out of the particle-bed. This requires that the distance of the print nozzle to the particle bed is as well increased, since it must be possible to move it across the reinforcement. The objective was thus to investigate the effect of that distance on print quality and to quantify a maximum allowable distance for an adequate print quality (for the printer setting used) in terms of shape accuracy and concrete strength. Compressive and flexural strength tests as well as geometrical measurements using a 3D scanning method were performed on specimen, printed with varying print nozzle to particle bed distances. It can be stated that for the used SPI print-heads, nozzle-types and parameter settings, the distance between the nozzle and the particle bed should not exceed 50 mm to ensure sufficient print quality in both shape accuracy and mechanical strength.

Keywords: Additive Manufacturing, Selective Paste Intrusion, Print Quality, Print Nozzle to Particle Bed Distance, Shape accuracy, 3D scanning

1. Introduction

The Selective Paste Intrusion (SPI) process is an additive manufacturing method to produce concrete elements. This process consists of two multiple repeated process steps, the deposition of a layer of aggregates in a particle bed followed by the selective binding with penetrating cement paste. The surrounding unbound aggregates thereby act as support structure for the built concrete element. This allows for the production of complex and free-form geometries without the need for a conventional formwork. The structure is then cured in the particle bed and can subsequently be excavated [1, 2].

Large attention is given to the reinforcement strategies for additive manufacturing in construction [3–7]. Among others, the Wire and Arc Additive Manufacturing (WAAM) is mentioned as a suitable method to reinforce concrete elements. In WAAM a steel wire is melted with an arc welder and applied in layers [8]. This process is intended to be integrated into the SPI process to create reinforced concrete elements with free-form geometries [9, 10] see Fig. 1

Preprints (www.preprints.org) | NOT PEER-REVIEWED | Posted: 13 March 2023 doi:10.20944/preprints202303.0236.v1

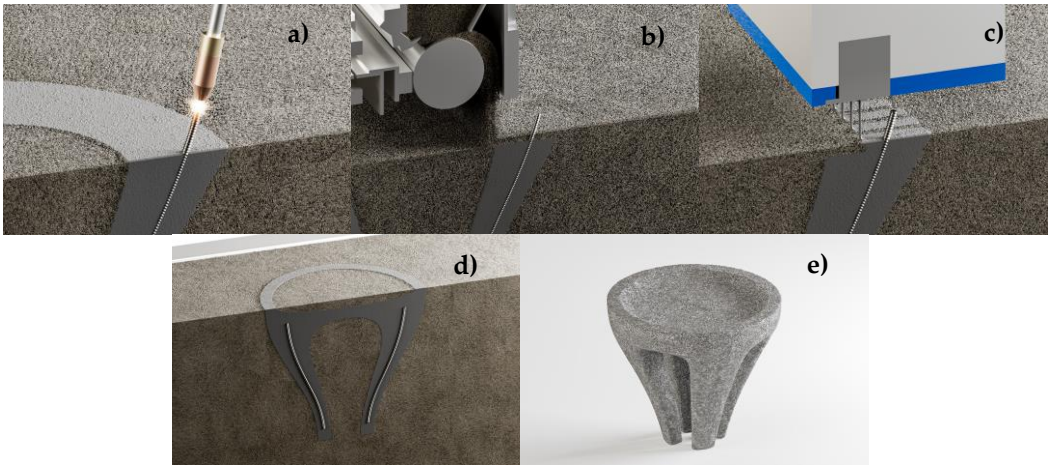

Figure 1: Combined SPI and WAAM process. a) printing a rebar, b) spreading an aggregate layer, c) cement paste application, d) curing of the finished reinforced concrete element, e) excavated component

Therefore, initial investigations on bond strengths between WAAM reinforcement and concrete compared to conventional reinforcing steel have already been undertaken [11]. However, the high temperatures generated by WAAM can adversely affect the rheological properties of the cement paste and potentially lead to deterioration in the hardened concrete in terms of mechanical properties [9, 12, 13]. Various cooling strategies, such as incorporate silica bonded water (dry water) in a granular bulk material (e.g. quartz sand) or active cooling by compressed air or water fog, are subject of current research [14]. But also passive cooling strategies by an increase of the distance between particle bed and welding spot [9, 15].

Previous studies have shown and quantified that the temperature in WAAM produced steel bars decreases with increasing distance from the welding spot [9, 15]. To reduce heat transfer into the particle bed, the distance between the welding spot and the particle bed has thus to be maximized. However, this simultaneously requires that the distance of the print nozzle to the particle bed is as well increased, since it must be possible to move the print head across the reinforcement. On the other hand, increasing that distance can lead to a decreased print quality of the SPI made concrete elements illustrated by both deteriorated shape accuracy and strength of the built elements.

This study aims to find an optimum between these two contradictory requirements. A maximum permissible distance for most efficient passive cooling (reduction of heat transfer into the particle bed), which at the same time also ensures a sufficient print quality has to be found.

2. Materials and Methods

2.1 Materials and production of the specimen

For concrete production, a quartz sand with a particle size 1.0-2.2 mm was used as aggregate in the particle bed. For the cement paste, an ordinary Portland cement was mixed with water (water-to-cement ratio of 0.35). In addition, a superplasticizer was used to ensure almost constant flow properties (mini-slump flow between 400 mm and 410 mm) of the cement paste over the complete printing time and for each test series (i.e. every selected nozzle to particle bed distance). For further strength testing, specimens with dimensions of 60 x 60 x 200 mm^3 were manufactured using the SPI method, see Fig. 2.

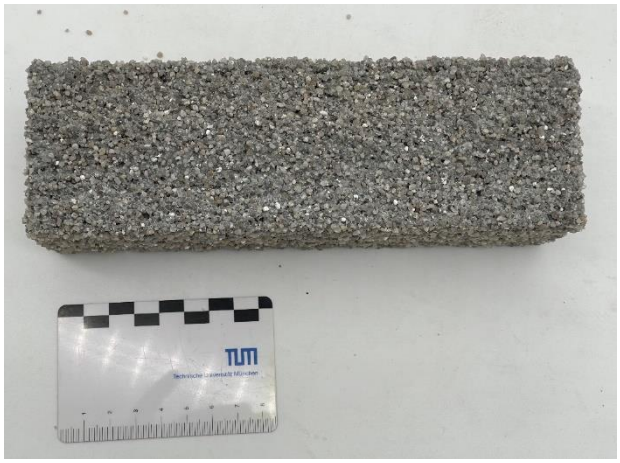

Figure 2: SPI printed specimen with designed dimensions of 60 x 60 x 200 mm³

Eight specimen were produced for each selected distance between the printing nozzle and the particle bed. The selected distances ranged from 20 mm to 80 mm with 10 mm increments. The test specimens were removed from the printer one day after production and were afterwards stored in a climate chamber at 20°C and 65 % relative humidity until testing.

2.2 Geometrical analysis

For scan data evaluation, each SPI specimen was scanned twice (once from each side, see Fig. 3 a) and b) respectively). A hand-held 3D scanner (Creaform HandySCAN Black Elite with an accuracy of 20 µm/m) was used for this purpose. To combine both scans of the SPI specimen , a point cloud alignment process, developed by [16], was used. Here, the point cloud distance of both scans was minimized with an iterative closest point (ICP) algorithm [17]. Ultimately, the alignment process results in a point cloud of the complete specimen, see Fig. 3 c).

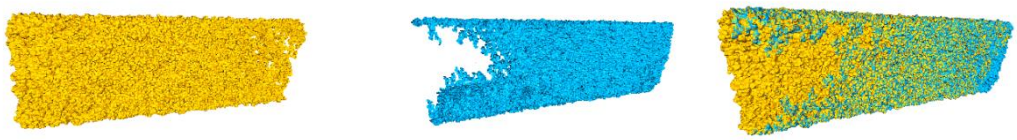

a) **b)** **c)**

Figure 3: Illustration of the a) first and b) second scan of an SPI sample. Both scans were combined, resulting in the c) complete scan of the sample.

Additionally, a point cloud of the design geometry of the SPI prisms was generated. Each plane of the prism consists of a grid with a point distance of 0.2 mm, see Fig. 4.

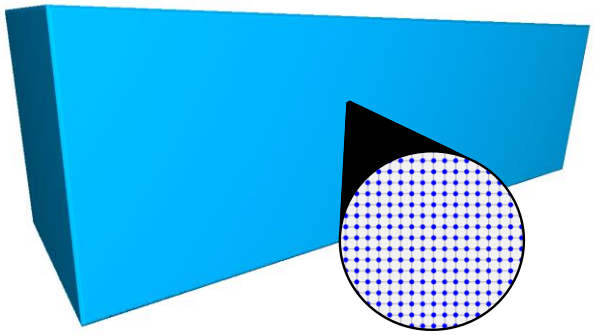

Figure 4: Visualization of the design prism geometry. The zoomed-in area demonstrates the planes consisting of a grid of 3D coordinates with a uniform point distance of 0.2 mm.

For a comparison between the geometry as per design and the actual built geometry of the printed sample (design-to-built comparison), both point clouds (combined SPI scan and the designed prism) were aligned, analogously to the aforementioned scan combination process. The voxel size describes the most affecting parameter of this procedure. It can be explained as a threshold of acceptance between the point cloud distances of the designed and actual geometries.

Increasing the voxel size allows for the alignment of point clouds with a high degree of differences. Ultimately, the alignment process results in a transformation matrix, relocating the SPI scan onto the designed prism. Fig. 5 visualizes the alignment of the designed prism (Fig. 5 a) and the combined SPI scan (Fig. 5 b), ultimately overlapping both geometries (Fig. 5 c).

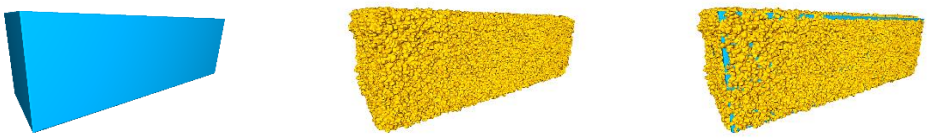

a) **b)** **c)**

Figure 5: a) Designed prism and the b) combined SPI scan are being aligned, resulting in a c) visualization of both geometries being overlaped.

Aim of the geometrical analysis was to determine the deviation between the designed and the built geometry for each plane individually. Therefore, the planes of the geometries needed to be segmented. In case of the prism as per design, each 3D coordinate within the same plane shares the same normal vector. This would allow a simple way of plane segmentation by clustering of normal vectors. Due to the rough surface of the SPI prisms, a regular plane segmentation via clustering of plane normal vectors could not be used for this application.

Therefore, the individual planes of the prism were separated with a sector-based approach. This means that the design prism was separated into sectors at first. The coordinates of the scanned samples were then assigned to their corresponding sector. In this paper, the sectors and planes of the prisms are referred to as left, right, front, back, top, and bottom. For each plane, a pyramid/trapezoid-shaped sector was constructed, generated by the angle bisectors of the designed prism geometry, see Fig. 6. The 3D coordinates of the SPI sample within a sector belong to their corresponding plane.

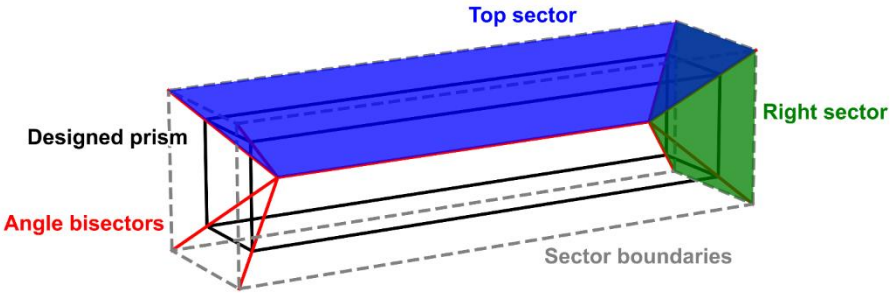

Figure 6: Visualization of the top sector (blue) and right sector (green), constructed with the angle bisectors (red) of the designed prism geometry (black lines). The dashed grey lines represent the boundaries of the sectors.

Fig. 7 conceptually illustrates the cross section of a corner segment of an SPI sample (blue and green dots) aligned with the designed prism geometry (black lines). The angle bisector (red line) of the horizontal top and vertical right plane divides the cross section into two sectors. Each coordinate of the SPI sample within the horizontal plane sector corresponds to the horizontal plane, each dot within the vertical plane sector to the vertical plane, respectively.

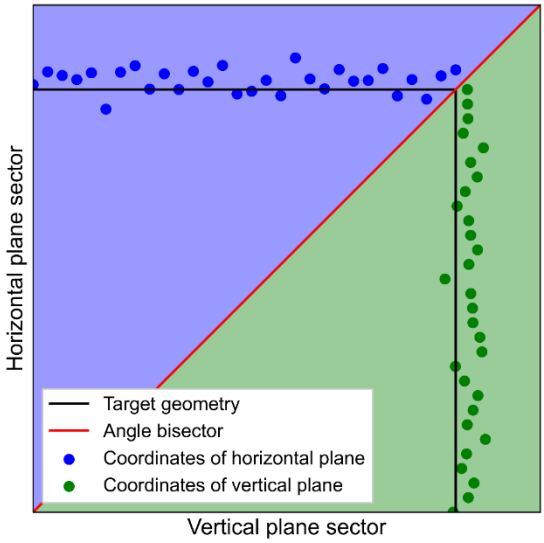

Figure 7: Concept of the plane segmentation with the constructed sectors. Coordinates of the SPI sample within the horizontal plane sector are assigned to the horizontal plane, coordinates within the vertical plane sector are assigned to the vertical plane.

Analogously to [16], the original coordinates of the SPI scan were aligned to a uniformed grid via nearest neighbor approximation. This allows the calculation of the surface area and the prism volume without surface triangulation. The original algorithm assumes a horizontal base for volume calculation [16]. Here, the base of each sector is represented by the tilted planes of the angle bisectors (see Fig. 6). Therefore, an additional grid was generated for the planes of the angle bisectors. As a result, the volume of each segmentation sector was calculated by the sum of all truncated prisms within.

The total volume of the SPI sample is the sum of all sector volumes. Fig. 8 shows the concept of the formation of the truncated prisms of the horizontal top plane and the vertical right plane for three grid rows. The surface area of the SPI specimens was calculated by the sum of all surface grid areas. Each grid segment is represented by two triangles [16]. Finally, the deviation of each plane of the SPI sample to the designed prism was calculated by determining the shortest distance of each coordinate of the SPI sample to their corresponding design plane. The final results are displayed in Fig. 9.

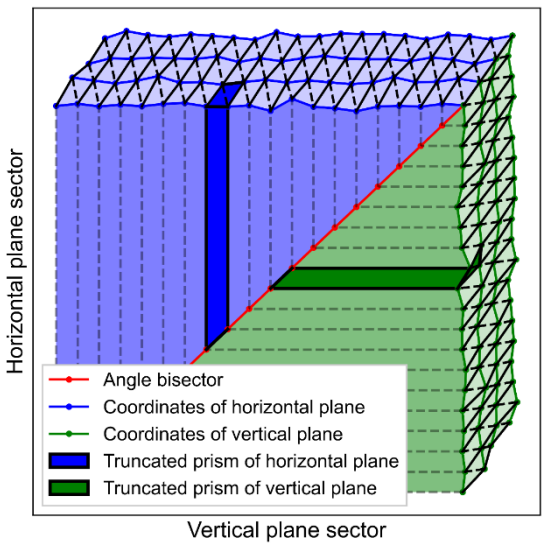

Figure 8: Formation of the truncated prisms used for volume and area calculation.

2.3 Strength testing

After scanning the specimen and one week before testing, five specimen per series were cut and grinded to conform to the dimensions of 40 x 40 x 160 mm3 according to DIN EN 196-1 [18]. This step is necessary as the surface of the SPI test specimens is uneven and the parallelism required can only be achieved through appropriate post-processing. After post-processing, the specimens were stored in the climate chamber at 20°C and 65 % r.H. again until testing. Compressive and flexural strength tests according to [18] were performed at an concrete age of 28 days.

3. Results and Discussion

3.1 Geometrical analysis

Fig. 9 shows the evaluation of the geometry on the side surfaces. It was evaluated how much the printed geometry deviates from the designed geometry for the different printing nozzle to particle bed distances investigated. Positive deviation values indicate that the measured coordinates are outside of the design geometry, meaning that the specimen is larger than the design at the measured location. On the other hand, negative deviation values indicate coordinates inside the design geometry, meaning that the specimen is smaller than the design at the measured location. This can be compared to Fig. 7.

It can be seen that as the distance increases, the deviation from the designed geometry as well increases (the value range becomes wider), and the values shift towards a negative deviation. The reason for the shift to smaller, partly negative deviation values is due to defects on the surface. The size of the samples does not change; instead, the surface becomes more irregular. These defects result in larger deviation range and peaks with negative values. The deviations of the test specimens with a low nozzle distance (20 mm, 30 mm and 40 mm) are in the positive deviation range between 0.25 mm and 2.0 mm.

It can thus be concluded that the test specimens with 20 mm, 30 mm and 40 mm nozzle distance have uniform shape accuracy in terms of geometry (low deviation values), but tend to be slightly larger than designed (deviation between +0.25 mm and +2.0mm). The specimen with an increased nozzle distance (above 50 mm) tend to be shifted to zero and even negative values. This means that these distances lead to larger irregularities (high scatter) and missing areas at the surface (negative deviation values). For geometrical accuracy, a nozzle to particle bed distance of 50 mm is thus recommended.

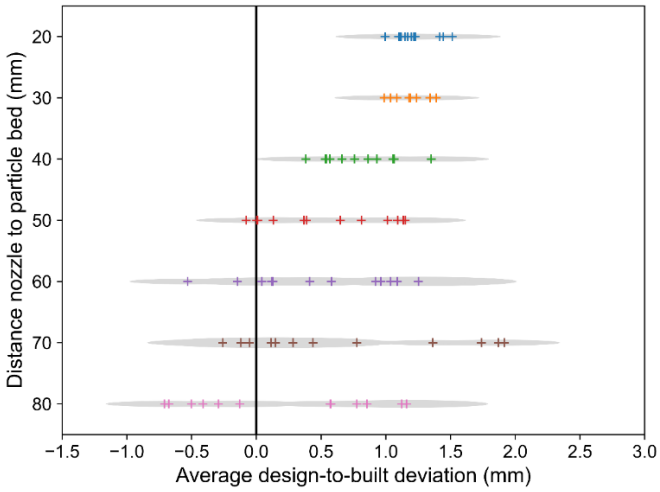

Figure 9: Geometrical analysis of specimen, printed with stepwise increased nozzle to particle bed distance. Increasing the distance results in increasing shape deviations

The fact that the SPI printer takes coordinates from the 3D model and applies the cement paste along this path means that the geometry of the applied cement paste in the particle bed is correct, but it is likely that aggregates at the surface are also bound, which

extend outside the nominal geometry bound by the cement Paste. Thus, it is conceivable that in the SPI process the geometric deviation is almost equal to the used maximum particle size in the particle bed, compare Fig. 7 and Fig. 9.

3.2 Strength testing

Fig. 10 shows that both, the compressive and the flexural concrete strength decrease with increasing the nozzle to particle bed distance. At a nozzle distance of only 20 mm, compressive strengths of about 60 MPa were achieved. At the maximum investigated distance of 80 mm, only two thirds of this value could be obtained (40 MPa), see Fig. 10. The flexural strength tests resulted in strengths between 7.9 MPa and 6.7 MPa at nozzle distances of 20 mm and 80 mm, respectively, see Fig. 10. This equals to a significant decrease of about 23%.

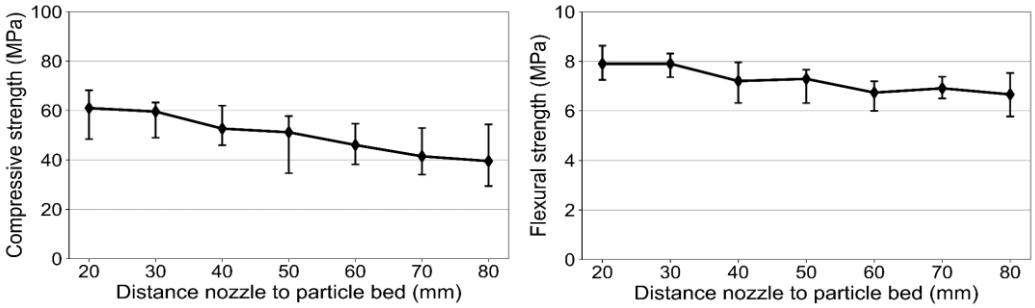

Figure 10: Mechanical performance analysis. Decreasing strength values with increasing nozzle to particle bed distance.

A Possible cause for the decreasing strength values with increasing nozzle distance are nozzle imperfections. Through imperfections, the cement paste stream, which should ideally hit the particle bed surface orthogonally, is deflected. The impact of the deflection increases with increasing nozzle distance and has a negative effect on the print quality. The deflection can cause defects as well as zones with unbound material within the test specimen.

Fig. 11 illustrates such imperfections of individual nozzles. Two figures show the nozzles from an orthogonal view to the printing direction (left), while the other two figures show the nozzles along the printing direction (right). For each view, a nozzle with the aspired flow direction (perpendicular stream of cement paste) is visible. In addition, each view exemplarily depicts a nozzle with a deviation of the cement paste stream.

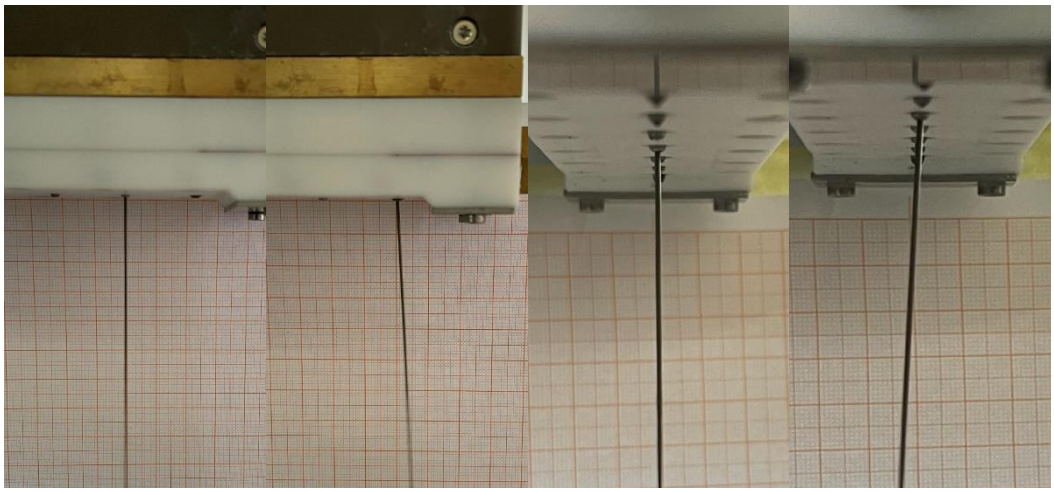

Figure 11: Different deflections of cement paste stream at different printing nozzles. Two figures show the orthogonal view to the printing direction (left), two figures show the view along the printing direction (right)

The resulting defects in the SPI element can already be detected during paste application to the particle bed. Where no negative effects of the nozzle imperfections can be seen at a nozzle distance of only 20 mm (Fig. 12), these effects are very evident at a nozzle distance of 80 mm (Fig 13).

Figure 12: Cement paste distribution at 20 mm

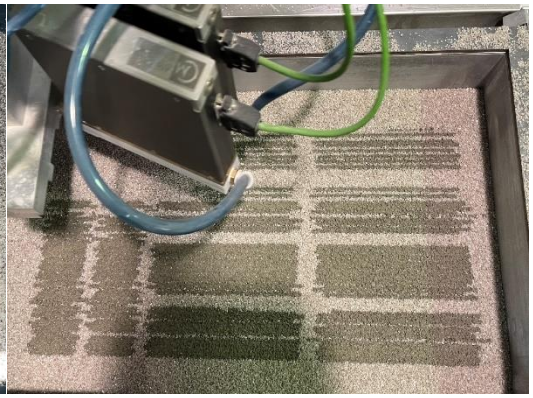

Figure 13: Cement paste distribution at 80 mm

Furthermore, Fig. 14 and Fig. 15. also shows post-processed test specimens (nozzle distances of 20 mm (Fig. 14) and 80 mm (Fig. 15)) before strength testing. The defects on the grinded surfaces are clearly visible for the specimen with increased nozzle distance.

Figure 14: Post-processed specimen (20 mm) before strength tests. Few voids and imperfections.

Figure 15: Post-processed specimen (80 mm) before strength tests. Major voids and imperfections.

It is noticeable that the strength values have strong fluctuations. For the compressive strengths, the values sometimes scatter over 20 MPa between the highest and lowest values at the same distance. For the flexural strengths, the scatter is in some cases up to 2.0 MPa. Possible causes for the high deviations in the strength values are:

- The potential presence of defects in the test specimens caused by clogged nozzles during the SPI process. During the SPI process, it occasionally happens that a printer nozzle gets clogged. This results in a lack of cement paste being applied at that spot, creating a defect in the test specimen. Since the material is not bonded at that spot, the structure is weakened, resulting in reduced strength. Voids and imperfections of process errors can be seen in Fig. 14.
- Inaccuracies in the post-processing of the specimens, such as not achieving parallelism, can lead to stress concentrations and the specimens failing at lower loads. The examination of the specimens after testing showed that the specimens with the highest deviation in parallelism also failed at lower loads during testing.

However, the declining trend in the strength values of both compressive and flexural strength indicates that the print quality decreases with increasing nozzle distance. The main reason for the decrease in strength lies in the imperfections of the printing nozzles, which were observed during the printing process, see Fig. 11 to Fig. 15.

Based on these findings, it is recommended to use a maximum distance of 50 mm in combination with WAAM between the printing nozzle and the particle bed to achieve the optimal balance between mechanical properties and print quality. This ensures both sufficient strength and high accuracy in the geometrical dimensions (see section 3.1). These findings are specific to the combination of our printer, the selected printing settings, and the material used. Therefore, caution should be taken when extrapolating these results to other printers, settings, or materials, as the outcomes may differ. However, it is worth noting that the observed trend in mechanical properties and print quality is likely to hold true for similar printing systems.

4. Conclusion and Outlook

This study shows that the deviation values of the geometrical analysis increases with increasing nozzle-distance. In other words contour precision decreases with increasing nozzle distance. The test specimens with nozzle distances of 20 mm, 30 mm, and 40 mm exhibit positive deviations ranging from 0.25 mm to 2.0 mm. This indicates that the specimens have consistent shape accuracy with low deviation values but are slightly larger than targeted (+0.25 mm to +2.0 mm). In contrast, specimens with nozzle distances above 50 mm tend to shift towards zero or negative values, indicating greater irregularities and missing areas on the surface.

In addition, the compressive and flexural strength of SPI-printed concrete specimen decrease as the distance between the printing nozzle and the particle bed increases. The highest compressive strength values of about 60 MPa were achieved at a minimum nozzle distance of 20 mm, while the lowest strength values of about 40 MPa were obtained at a distance of 80 mm. The flexural strength values follow this trend. Furthermore, a high standard deviation in the strength values was observed which could mainly be attributed to imperfections in the specimen post-processing.

Main reason for the increasing geometrical deviations and decrease in strength with increasing nozzle to particle bed distances was found in imperfections in the nozzle, and the resulting deflection of the cement paste stream. The high standard deviation in strength values may be attributed to the presence of defects in the test specimens due to clogged nozzles during the SPI process and inaccuracies in post-processing. However, despite these sources of error, the trend of decreasing strength values with increasing nozzle distance is evident and therefore these sources of error do not significantly impact the overall results.

In summary, this study has investigated the effects of increasing the distance between the printing nozzle and the particle bed in the Selective Paste Intrusion (SPI) process on the mechanical properties and geometrical shape accuracy of test specimens. According to the results, the mechanical properties decrease and the deviation of geometry increases as the distance between the printing nozzle and particle bed increases.

A significant decline in these properties occurs beyond a distance of 50 mm. Therefore, it is recommended to maintain a distance of maximum 50 mm between the printing nozzle and the particle bed when using Wire Arc Additive Manufacturing (WAAM) with our specific printer, materials, and selected printing settings. It is important to note that these findings may differ if any of these parameters are changed. Nonetheless, limiting the distance to within this range should provide the optimal balance between mechanical properties and print quality with our current setup.

Further research should focus on identifying strategies, such as active cooling systems, to mitigate the negative effects of temperature on the cement paste near the reinforcing bars produced by the WAAM process.

Funding

This research was funded by the Deutsche Forschungsgemeinschaft (DFG, German Research Foundation) – Project-number 414265976 – TRR 277

Acknowledgement

The authors would like to thank Philip Schneider, Chair of Materials Science and Testing, Technical University of Munich, for the support with the renderings of Fig. 1.

References

[1] Weger, D., Gehlen, C., Lowke, D. Additive Fertigung von Betonbauteilen durch selektive Zementleim-Intrusion. *Proceedings of Ibausil* 2018.

[2] Weger, D. 2020. *Additive Fertigung von Betonstrukturen mit der Selective Paste Intrusion – SPI / Additive manufacturing of concrete structures by Selective Paste Intrusion - SPI. Dissertation*, Munich.

[3] Freund, N., Dressler, I., and Lowke, D. 2020. Studying the Bond Properties of Vertical Integrated Short Reinforcement in the Shotcrete 3D Printing Process. In *Second RILEM International Conference on Concrete and Digital Fabrication*, F. P. Bos, S. S. Lucas, R. J. Wolfs and T. A. Salet, Eds. RILEM Bookseries. Springer International Publishing, Cham, 612–621. DOI=10.1007/978-3-030-49916-7_62.

[4] Hass, L. and Bos, F. 2020. Bending and Pull-Out Tests on a Novel Screw Type Reinforcement for Extrusion-Based 3D Printed Concrete. In *Second RILEM International Conference on Concrete and Digital Fabrication*, F. P. Bos, S. S. Lucas, R. J. Wolfs and T. A. Salet, Eds. RILEM Bookseries. Springer International Publishing, Cham, 632–645. DOI=10.1007/978-3-030-49916-7_64.

[5] Kloft, H., Empelmann, M., Hack, N., Herrmann, E., and Lowke, D. 2020. Reinforcement strategies for 3D-concrete-printing. *Civil Engineering Design* 2, 4 (2020), 131–139. DOI=10.1002/cend.202000022.

[6] Matthäus, C., Kofler, N., Kränkel, T., Weger, D., and Gehlen, C. 2020. Interlayer Reinforcement Combined with Fiber Reinforcement for Extruded Lightweight Mortar Elements. *Materials (Basel, Switzerland)* 13, 21 (2020). DOI=10.3390/ma13214778.

[7] Mechtcherine, V., Buswell, R., Kloft, H., Bos, F. P., Hack, N., Wolfs, R., Sanjayan, J., Nematollahi, B., Ivaniuk, E., and Neef, T. 2021. Integrating reinforcement in digital fabrication with concrete: A review and classification framework. *Cement and Concrete Composites* 119 (2021), 103964. DOI=10.1016/j.cemconcomp.2021.103964.

[8] Rodriguez, N., Vázquez, L., Huarte, I., Arruti, E., Tabernero, I., and Alvarez, P. 2018. Wire and arc additive manufacturing: a comparison between CMT and TopTIG processes applied to stainless steel. *Weld World* 62, 5, 1083–1096. DOI=10.1007/s40194-018-0606-6.

[9] Weger, D., Baier, D., Straßer, A., Prottung, S., Kränkel, T., Bachmann, A., Gehlen, C., and Zäh, M. Reinforced Particle-Bed Printing by Combination of the Selective Paste Intrusion Method with Wire and Arc Additive Manufacturing – A First Feasibility Study 28, 978–987. DOI=10.1007/978-3-030-49916-7_95.

[10] Riegger, F. and Zäh, M. F. 2022. Additive Fertigung von Stahlbewehrungen. *Zeitschrift für wirtschaftlichen Fabrikbetrieb* 117, 7-8 (2022), 448–451. DOI=10.1515/zwf-2022-1091.

[11] Tischner, K., Rappl, S., Riegger, F., Straßer, A., Osterminski, K., Kränkel, T., Baehr, S., Zaeh, M. F., and Gehlen, C. Bond Behavior of WAAM Reinforcements in Comparison to Conventional Steel Reinforcements. *Construction Materials (under review)* 2023.

[12] Straßer, A., Niewöhner F., and Kränkel, T. 2023. Effect of Temperature Loads in the Fresh State on the Flexural and Compressive Strength of Concrete. cbm - Centrum Baustoffe und Materialprüfung. https://media-tum.ub.tum.de/doc/1701171/1701171.pdf.

[13] Straßer, A., Weger, D., Matthäus, C., Kränkel, T., and Gehlen, C. 2022. Combining Wire and Arc Additive Manufacturing and Selective Paste Intrusion for Additively Manufactured Structural Concrete. *Open Conf Proc* 1 (2022), 61–72. DOI=10.52825/ocp.v1i.75.

[14] Hamilton, L. D., Zetzener, H., and Kwade, A. 2022. The Effect of Water, Nanoparticulate Silica and Dry Water on the Flow Properties of Cohesionless Sand. *Processes* 10, 11 (2022), 2438. DOI=10.3390/pr10112438.

[15] Straßer, A., Riegger, F., Hamilton, L. D., Kränkel, T., Gehlen, C., Zaeh, M. F., and Kwade, A. Selective Paste Intrusion: Integration of Reinforcement by WAAM — Concept and Overview of the Current Research. *Preprints* 2023, 2023030260. DOI=10.20944/preprints202303.0260.v1.

[16] Haynack, A., Timothy, J. J., Kränkel, T., and Gehlen, C. 2022. *Characterization of Cementitious Materials Exposed to Freezing and Thawing using 3D Scans*.

[17] Rusinkiewicz, S. and Levoy, M. 2001. Efficient variants of the ICP algorithm. In *Proceedings / Third International Conference on 3-D Digital Imaging and Modeling. 28 May - 1 June 2001, Quebec City, Canada*. IEEE Computer Soc, LosAlamitos, Calif., 145–152. DOI=10.1109/IM.2001.924423.

[18] DIN Deutsches Institut für Normung e.V. *DIN EN 196-1:2016-11. Methods of testing cement – Part 1: Determination of strength*. Beuth, November 2016.